Stimulated emission in the heavily doped $Al_{0.68}Ga_{0.32}N:Si$ structures with transverse optical pumping at room temperature

© P.A. Bokhan[1], K.S. Zhuravlev[1], D.E. Zakrevsky[1,2], T.V. Malin[1], I.V. Osinnykh[1,3], N.V. Fateev[1,3]

[1] Rzhanov Institute of Semiconductor Physics, Siberian Branch, Russian Academy of Sciences,
630090 Novosibirsk, Russia
[2] Novosibirsk State Technical University,
630073 Novosibirsk, Russia
[3] Novosibirsk State University,
630090 Novosibirsk, Russia

E-mail: fateev@isp.nsc.ru

Received November 21, 2022
Revised December 16, 2022
Accepted December 22, 2022

The broadband stimulated emission in the spectral range $\lambda = 380-700$ nm with the inhomogeneous broadening has been experimentally obtined in the heavily doped $Al_{0.68}Ga_{0.32}N:Si$ structures grown by molecular beam epitaxy. The behavior of the intensities and spectra of stimulated emission from the edge of the active element with transverse pulsed pumping by radiation with $\lambda = 266$ nm, measured at room temperature, demonstrate the threshold behavior and optical gain. For stimulated emission with a maximum at $\lambda = 500$ nm, the minimum threshold pump power density was 6.5 kW/cm^2 for excited region length of 1.5 mm. The parameters and contributions of the two main processes $e-A$ and $D-A$ of radiative recombination in the excited structures for stimulated emission and optical gain are studied.

Keywords: stimulated emission, heavily doped $Al_xGa_{1-x}N$ structures, luminescence, optical gain, donor-acceptor recombination.

DOI: 10.21883/SC.2022.12.55148.4349

1. Introduction

The issue of production of high-intensity, efficient, long-lived, and compact semiconductor light sources of different spectral ranges remains topical. This also applies to the generation of broadband visible radiation and narrow lines of laser radiation with continuous tuning of the generation frequency within a wide spectral range. Such devices have numerous possible applications (specifically, they may be used as energy-efficient, durable, and environmentally friendly radiation sources with a continuous spectrum and laser sources with high luminous and energy efficiencies).

The use of wide-gap A_3-nitride semiconductors in optoelectronic and electronic devices was a significant step forward in the design of instruments of this kind. For example, InGaN/GaN heterostructures for blue laser diodes have been fabricated in 1996 [1]. The technique of fabrication of light-emitting devices based on edge emission in InGaN structures in the $\lambda = 400-460$ nm spectral range has advanced considerably since then, and they have entered mass production. However, much-needed efficient sources of green light ($\lambda = 530-560$ nm, which corresponds to the maximum sensitivity of human eyes) have not been realized yet. This may be done by increasing the indium concentration. However, it is very difficult to grow low-defect structures of this kind with a good optical quality, and the efficiency of light-emitting devices takes a catastrophic hit [2–5].

Wide-gap $Al_xGa_{1-x}N$ structures, which are currently regarded as promising materials for compact and efficient light-emitting and laser diodes of the ultraviolet range [6–8], may provide a solution to this problem. Varying x, one may alter bandgap width E_g within the range of 3.4–6.2 eV ($\lambda = 200-365$ nm). When $Al_{0.68}Ga_{0.32}N$ structures are doped with, e.g., silicon with concentration $n_{\text{Si}} > 10^{19}$ cm^{-3}, dominant broadband ($\lambda = 380-700$ nm) emission with quantum efficiency $\eta \geq 0.57$ emerges in the spectrum [9]. This makes them promising media for both broadband light sources and lasers operating throughout almost the entire visible range and, possibly, providing a wide tuning range of the emission frequency of an single emitting element.

The aim of the present study is to examine experimentally the parameters of stimulated emission (SE) in heavily doped $Al_{68}Ga_{32}N:Si$ structures under transverse optical pumping at $\lambda = 266$ nm at room temperature.

2. Experiment procedure

The studied $Al_xGa_{1-x}N:Si$ structures were grown by molecular beam epitaxy technique. Ammonia and a mixture of silane SiH_4 and nitrogen served as sources of active nitrogen and dopant Si atoms, respectively. Films with thickness $h = 1.2\,\mu$m were grown on (0001) nitrided sapphire substrates with a thickness of 0.43 mm at a temperature of 860°C and an ammonia flow of 130 cm^3/min under a total mixture pressure of $5 \cdot 10^{-5}$ Torr. Buffer AlN films with a thickness of 350 nm were grown preliminary on these sapphire substrates. The procedure of synthesis and measurement of characteristics of AlGaN films was

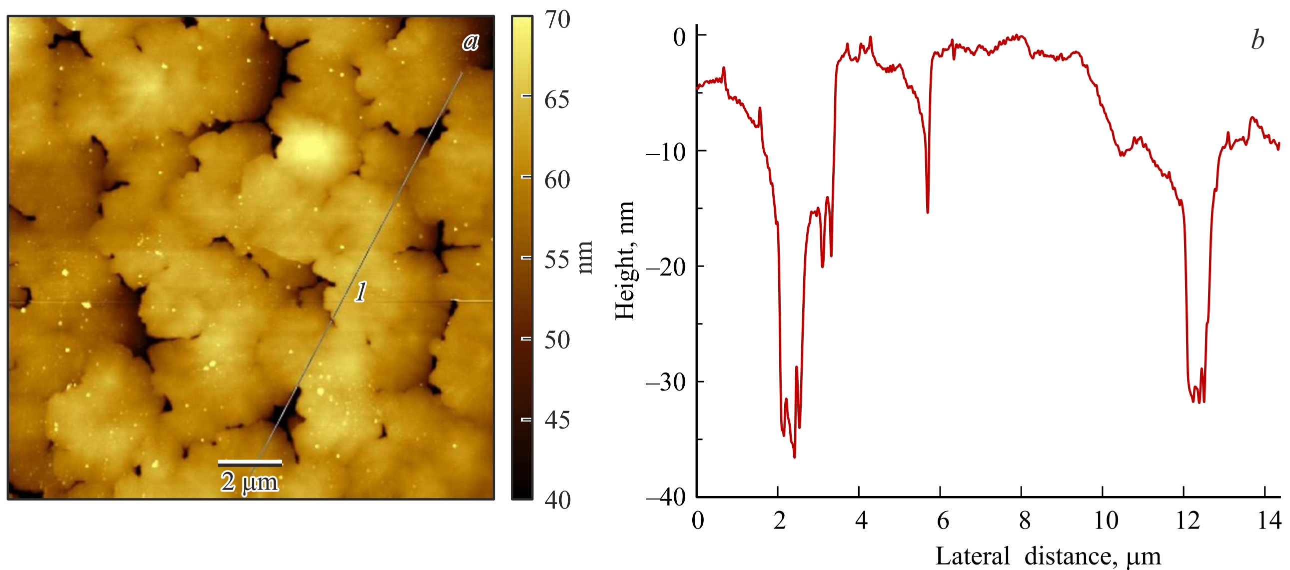

Figure 1. Surface morphology of the $Al_{0.68}Ga_{0.32}N:Si$ structure: *a* — AFM image of the surface, *b* — profile of scan along line *1*.

detailed in [10]. The densities of dopant Si atoms measured by secondary-ion mass spectrometry vary with depth from $n_{Si} = 1.7 \cdot 10^{20}$ to $7 \cdot 10^{18}\,cm^{-3}$. The densities of oxygen and carbon atoms are $3 \cdot 10^{18}\,cm^{-3}$ and $4 \cdot 10^{18}\,cm^{-3}$, respectively.

To actually produce efficient light sources, one needs to fabricate AlGaN:Si structures with a low level of optical losses on the active element, a low density of defects, and a smooth surface. Due to the lack suitable cleavage faces, edges of structures were polished with a diamond sandpaper with < 500 nm grains. Images of polished edges obtained using an optical microscope revealed excelent optical properties of the surface. The coefficient of radiation reflection from the edge under normal incidence is ~ 0.14, since the refraction index of $Al_{0.68}Ga_{0.32}N$ is $n = 2.2$ at $\lambda = 500$ nm [11]. An atomic force microscope (AFM) was used to study the surface morphology of the structure.

The image of the surface of AlGaN layers with an area of $15 \times 15\,\mu m^2$ (Fig. 1, *a*) reveals six-sided hillocks $\sim 3{-}5\,\mu m$ in diameter; the root-mean-square (RMS) surface roughness is < 5 nm, which is indicative of a smooth morphology. However, while the roughness value is low, dimples up to 35 nm in depth, which form between hillocks (Fig. 1, *b*), are seen in the same image and introduce additional intra-waveguide radiation losses. Since the surface roughness value and the depth of dimples are small compared to the $Al_{0.68}Ga_{0.32}N$ film thickness, an low level of optical losses is to be expected.

Samples with a length of 15 mm and a width of 3 mm were used as active elements. Pulsed fourth-harmonic radiation of an Nd:YAG laser with wavelength $\lambda = 266$ nm, a repetition rate of 10 Hz, and a pulse duration of 8 ns provided transverse optical pumping. The pump radiation power was attenuated by neutral filters and calibrated dielectric mirrors. A pump beam was focused by a cylindrical lens with a focal distance of 10 cm into a uniform strip ($100\,\mu m$ in width and up to 1.5 mm in length) perpendicular to the surface from the $Al_{0.68}Ga_{0.32}N$ side (Fig. 2, *a*). The length of the excitation strip was set by adjusting the position of a screen, which could block pump radiation, by the microscrew with an accuracy of $5\,\mu m$. The luminescence intensity was measured from the excitation strip surface under an angle of 45° to its normal. Edge radiation of the structure (Fig. 2, *a*) reached a quartz light guide with a core diameter of 1 mm, the end of which was located at a distance of 4.5 mm from the edge of the structure. Radiation from the output of this light guide was received to a spectrometer with a resolution of 0.5 nm in the $\lambda = 250{-}800$ nm spectral range. This was the setup used to measure the emission spectrum. In a different arrangement, radiation was routed to the input of a monochromator with a spectral resolution of 10 nm. Output radiation from the monochromator output was fed to a photomultiplier, and the produced electric signal was recorded with a Tektronix TDS2024B oscilloscope. Temporal profiles of decay of emission intensity $I(t_k)$ after an excitation pulse were determined for fixed values of the emission wavelength and pump radiation power density P_p. A characteristic temporal curve of the stimulated emission intensity is shown in Fig. 2, *b*. The total area under these curves defines the relative overall intensity of stimulated emission within the time interval from 0 to t_m with time step $\Delta t = t_{k+1} - t_k = 1$ ns, which is given by [12,13]

$$I = \sum_{k=0}^{k=m} I(t_k)\Delta t. \quad (1)$$

Maximum measurement time $t_m \sim 30\,\mu s$ was chosen so as to correspond to the point when decaying $I(t_m)$ becomes comparable to the noise level. The temporal behavior of the output emission intensity is complex due to the

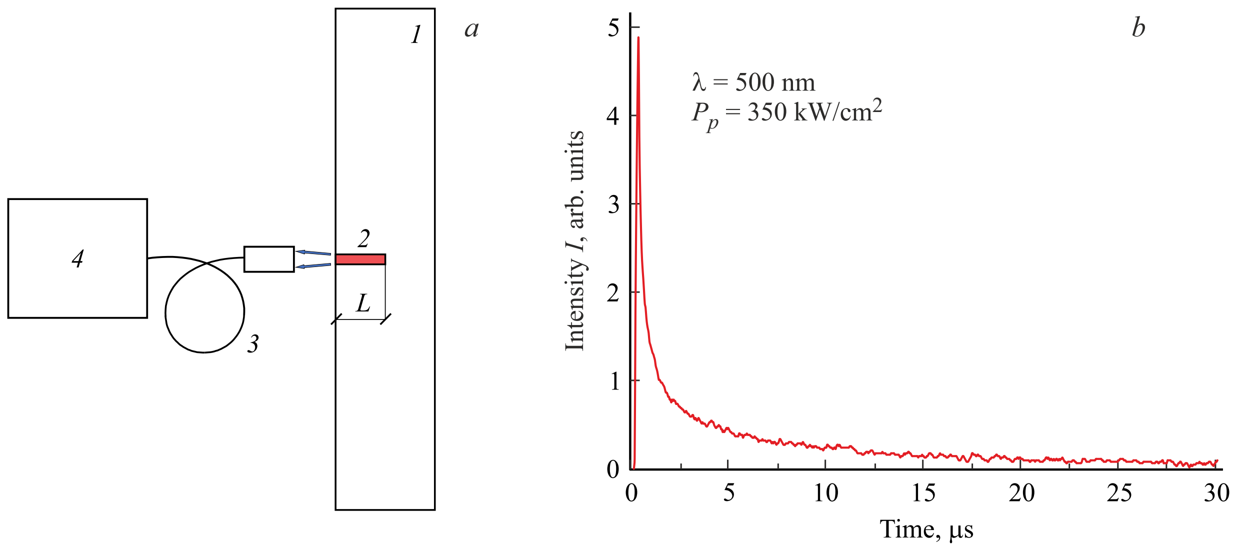

Figure 2. *a* — Diagram of the experiment: *1* — $Al_{0.68}Ga_{0.32}N$ structure, *2* — excitation strip, *3* — light guide, *4* — monochromator *b* — Temporal profile of decay of the stimulated emission intensity decay

presence of two major processes of radiative recombination in $Al_{0.68}Ga_{0.32}N:Si$ structures. These curves (see Fig. 2, *a*) feature fast (with exponential decay within several tens of nanoseconds) and slow (with hyperbolic decay within several microseconds) components [12]. These conclusions are verified by the results of approximation of experimental data by a sum of exponential and hyperbolic functions [13], which are used to determine the areas under these decay curves. The fast component is associated with electron–acceptor $(e{-}A)$ recombination, while the slow one corresponds to the recombination of donor–acceptor pairs $(D{-}A)$. The relative contributions of fast and slow components for the overall SE intensity and the optical gain coefficients were calculated based on these results. The absolute pump and SE powers were measured with a Thorlabs S401C sensor.

3. Results and discussion

Optical excitation of the active medium induces luminescence. If optical gain dominates over losses in radiation propagation along the excitation strip, SE is produced throughout almost the entire range of luminescence wavelengths with a non-uniform spectrum broadening. The intensity of SE generated under excitation of a strip with length L (Fig. 2, *a*) is characterized by the following formula [14]:

$$I(L) = (Is \cdot S/k_0)\left[\exp(k_0 \cdot L) - 1\right], \quad (2)$$

where I_s is the luminescence power density, S is the cross-section area of the excited region, $k_0 = (k_1 - \delta)$ is the experimentally observed optical gain coefficient, and k_1 and δ are the gain due to stimulated emission and the optical loss coefficient, respectively.

Figure 3 presents the dependences of overall intensity I on excitation strip length L for $\lambda = 500$ nm at two different pump power densities (P_p). A photographic image of the stimulated emission spot at a distance of 4.5 mm from the output edge of the structure with a uniform distribution (near-Gaussian in two transverse directions) is shown in the same figure. The initial section of the $I(L)$ dependence (solid curves in Fig. 3) is characterized well by formula (2), which is indicative of SE generation in the excited strip. These data allow one to determine the values of overall optical gain coefficient $k_0 = 325$ and $533\,\text{cm}^{-1}$ at pump power densities $P_p = 125$ and $500\,\text{kW/cm}^2$, respectively.

As the excitation region extends in length, intensity $I(L)$ reaches saturation, since a fraction of radiation from far sections is lost in propagation to the detector. Intensity $I(L)$ with the excitation strip positioned at an angle of 15° to the

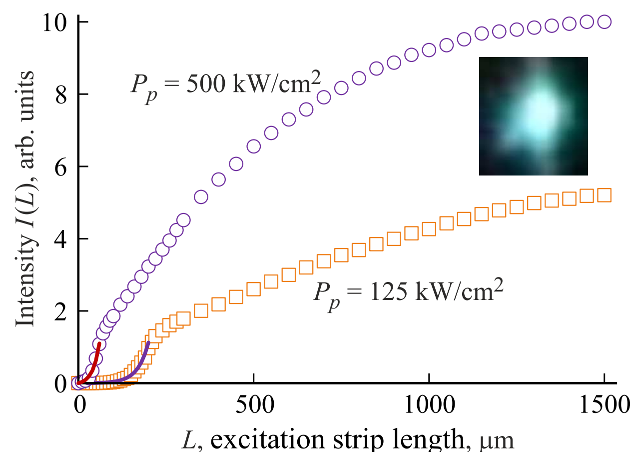

Figure 3. Dependences of output radiation intensity I on length L of the excitation region. A photographic image of the stimulated emission spot is shown in the inset.

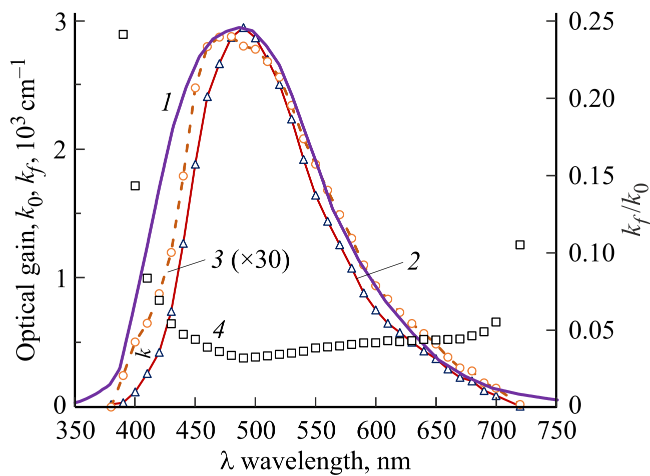

Figure 4. Normalized luminescence contour (*1*) and spectral dependences of overall optical gain coefficient k_0 (*2*); fast gain component k_f (*3*); and ratio k_f/k_0 (*4*) at $P_p = 200\,\text{kW/cm}^2$.

edge of the structure was determined in a separate series of measurements. The results did not differ from the ones obtained earlier. Therefore, reflection from the edge face under normal incidence does not affect the SE parameters.

It was demonstrated in [15,16] that the method of derivation of optical gain coefficients from the dependence of the emission intensity on the excitation region length is incorrect, since the radiation escape to the passive section of the structure is not taken into account. Another method for determining the optical gain coefficients was used in [12,17], where the gain for probe radiation intensity I_{pr} propagating through the excited structure was measured. The temporal behavior of intensity of probe radiation of an incandescent lamp transmitted through the structure with pump radiation present ($I^*(t)$) and intensity $I(t)$ without probe radiation were measured at fixed wavelengths and pump intensities. The value of $I_{st}(t) = I^*(t) - I(t)$ characterizes the behavior of stimulated emission produced in a single pass through the excited structure. Quantity $G(t) = \exp[k(t)h] = I_{st}(t)/I_{pr}$ is then the single-pass gain that allows one to determine the temporal behavior of optical gain coefficient $k(t)$. Processing the decay curves using formula (1), one may determine the values of overall optical gain coefficient $k_0 = k_f + k_s$ and fast k_f and slow k_s gain components. The measured overall gain is approximated well by linear function $k_0\,[\text{vm}^{-1}] = 16.9 \cdot P_p\,[\text{kW/cm}^2]$ [13] in the range of variation of pump power density through to $P_p = 1.2\,\text{MW/cm}^2$. The curve is nonlinear in the region of small values of $P_p < 100\,\text{kW/cm}^2$. Ratio k_f/k_0 of the fast gain component to the overall gain also increases at small P_p values.

Figure 4 presents the spectral dependences of overall optical gain coefficient k_0; fast gain component k_f; and ratio k_f/k_0. The luminescence spectrum, which is wider than the spectral dependences for optical gain coefficients, is also shown in this figure. A ~ 1.36-fold reduction in the gain spectrum width is associated with an exponential increase in the intensity of the inhomogeneously broadened luminescence spectrum.

The investigation of temporal dependences of the luminescence intensity and the SE intensity reveals the presence of two major processes of radiative recombination: a slow process (with a half-maximum duration of $\sim 2\,\mu$s) and a fast one (~ 70 ns).

The fast SE component is attributable to electron–acceptor ($e{-}A$) recombination, while the slow one corresponds to the recombination of donor–acceptor pairs ($D{-}A$ recombination) [12,13]. In contrast to SE with homogeneous broadening of the active medium, broad emission bands in $e{-}A$ and $D{-}A$ recombination processes form an inhomogeneously broadened spectral profile (due to the fact that distances between recombinating particles differ). The above-threshold behavior of intensity in inhomogeneously broadened media differs greatly from its behavior in media with a homogeneously broadened spectrum. Having reached a minimum near the generation threshold, the SE spectrum broadens again at higher pump intensities until it reaches the full inhomogeneous line width. This is attributable to the fact that saturation at the center of the emission spectrum does not suppress the gain in wings. The fast optical gain coefficient increases considerably at the edges of the spectral range, due likely to the spectrum for $e{-}A$ recombination being wider than the one for $D{-}A$ recombination. Overall optical gain coefficients $k_0 = 2100$ and $8400\,\text{cm}^{-1}$ for $P_p = 125$ and $500\,\text{kW/cm}^2$ determined in [13] are considerably higher than the values obtained in the present study. These results verify the conclusions made in [15,16].

Figure 5 presents dependences $I(P_p)$ of the overall edge SE intensity versus the pump power density for three different excitation strip lengths L. The $I(P_p)$ dependences are threshold in nature (see the inset in Fig. 5), thus verifying the generation of SE. The threshold pump power for $L = 0.5$, 1, and 1.5 mm is $P_{\text{th}} \approx 16.9$, 8.9, and $6.5\,\text{kW/cm}^2$, respectively. The output emission

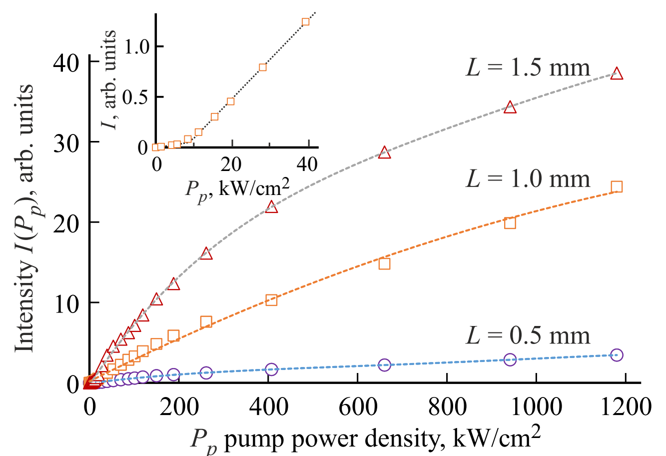

Figure 5. Dependences of stimulated emission I versus pump power density P_p. The initial $I(P_p)$ section for $L = 1$ mm is shown in the inset.

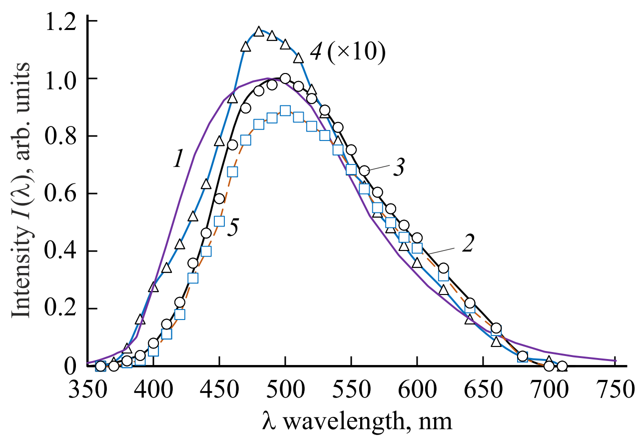

Figure 6. Normalized emission spectra $I(\lambda)$ at $P_p = 500\,\mathrm{kW/cm^2}$, $L = 1.5$ mm. *1* — Luminescence; *2* — stimulated emission (solid curve); *3* — stimulated emission derived from temporal dependences (circles); *4, 5* — fast and slow SE components, respectively.

intensity increases linearly in the above-threshold region ($P_p > P_{th}$). A sublinear growth of $I(P_p)$ is observed at $P_p > 200\,\mathrm{kW/cm^2}$ through to $P_p = 1200\,\mathrm{kW/cm^2}$. This may be attributed to a restriction on pump absorption established when the number of absorbed quanta becomes equal to the number of absorption centers.

Figure 6 shows the output emission spectra at pump power density $P_p = 500\,\mathrm{kW/cm^2}$. The broadest luminescence has half-width $\Delta\lambda = 153.8$ nm. Half-width $\Delta\lambda_{se}$ of SE spectra decreases due to the intensification of luminescence in propagation along the strip. As the excitation power increases from $P_p = 260$ to $940\,\mathrm{kW/cm^2}$, the value of $\Delta\lambda_{se}$ decreases monotonically from 144.6 to 130.7 nm. The half-width of spectra of fast SE components associated with the $e-A$ recombination process also decreases from 151.9 to 127.4 nm. The values of $\Delta\lambda_{se}$ of stimulated emission are large due to inhomogeneous broadening of the emission line for recombination processes.

Experimental results demonstrate that the SE pulse duration decreases relative to the luminescence duration. For example, the half-maximum durations of pulses for fast SE components with exponential decay decrease by a factor of ~ 1.3 and are independent of the pump power. The relaxation time for slow components with a hyperbolic temporal behavior becomes ~ 2 times shorter.

The measured fraction of pump energy converted into the SE energy (with one-way radiation propagation, $L = 1$ mm) is $\sim 7\%$. Although the quantum yield of luminescence is high, losses due to SE escape from the excited region in other directions are also high. A cavity matched with the excitation region may enhance the conversion efficiency considerably. Measurements revealed that luminescence and stimulated emission from the edge of the structure (and their fast and slow components) are non-polarized, which is typical of their recombination mechanisms.

The obtained experimental data and results of discussions regarding the mechanisms of radiative recombination in doped GaN structures [18] suggest the following model of radiative recombination. Owing to heavy doping with silicon, donor and acceptor levels in an AlGaN structure transform into broad bands that merge with the edges of the valence and conduction bands. Under equilibrium conditions with full compensation, electrons from donors (D) migrate to acceptors (A); therefore, D^+, D^0, and A^- centers are present in the bulk of the structure, while conduction is almost nonexistent. Non-equilibrium conditions are established due to ionization of A^- with the production of a free electron in the conduction band and a neutral acceptor as a result of optical pumping by radiation with quantum energy $E_{h\nu} = 4.66$ eV, which is smaller than the bandgap width of the $\mathrm{Al_{0.68}Ga_{0.32}N}$ structure ($E_g = 5.1$ eV), with an absorbed energy fraction of ~ 0.26. Thus, electrons from negatively charged acceptors A^- migrate to the conduction band and form electron–neutral acceptor pairs. In the course of subsequent thermalization, electrons may either return to neutral acceptors ($e-A$ recombination) or be captured by ionized donors and then recombine with holes at neutral acceptors ($D-A$ recombination) with the emission of a quantum. These two mechanisms are the major processes of radiative recombination in heavily doped structures. The cross section of capture of electrons by positively ionized dopant impurities D^+ is the greatest (up to $10^{-12}\,\mathrm{cm^2}$) [19], since the long-range Coulomb potential produces an additional attraction for electrons. The capture cross section for neutral impurities is $2-3$ orders of magnitude lower; therefore, the cross section of capture of an electron by a positively ionized donor is much higher than the cross section of capture of an electron by a neutral acceptor. Experimental data on the ratio of intensities of $D-A$ and $e-A$ recombination processes confirm the validity of this model.

4. Conclusion

Thus, stimulated emission within a wide spectral range ($\lambda = 380-700$ nm) was observed experimentally under transverse optical pumping of a heavily doped $\mathrm{Al_{0.68}Ga_{0.32}N:Si}$ structure at room temperature. The center of the stimulated emission line was at $\lambda \sim 500$ nm, and the excitation power density threshold for its generation was $P_p = 6.5\,\mathrm{kW/cm^2}$ at excitation strip length $L = 1.5$ mm. This low threshold is attributable to fine optical quality of the structure and its high optical gain coefficient. The obtained results show the feasibility of fabrication of diode lasers with a wide emission spectrum in the visible range.

Funding

This study was carried out under state assignment FWGW-2022-0012.

Conflict of interest

The authors declare that they have no conflict of interest.

References

[1] K. Itaya, M. Onomura, J. Nishio, L. Sugiura, S. Saito, M. Suzuki, J. Rennie, S. Nunoue, M. Yamamoto, H. Fujimoto. Jpn. J. Appl. Phys., **35**, L1315 (1996).
[2] S.F. Chichibu, A.C. Abare, M.P. Mack, M.S. Minsky, T. Deguchi, D. Cohen, P. Kozodoy, S.B. Fleischer, S. Keller, J.S. Speck, J.E. Bowers, E.Hu, U.K. Mishra, L.A. Coldren, S.P. DenBaars, K. Wada, T. Sota, S. Nakamura. Mater. Sci. Engin. B, **59**, 298 (1999).
[3] F.A. Ponce, S. Srinivasan, A. Bell, L. Geng, R. Liu, M. Stevens, J. Cai, H. Omiya, H. Marui, S. Tanaka. Phys. Status Solidi B, **240**, 273 (2003).
[4] W.V. Lundin, A.E. Nikolaev, A.V. Sakharov, E.E. Zavarin, S.O. Usov, V.S. Sizov, A.L. Zakgeim, A.E. Chernyakov, A.F. Tsatsul'nikov. Tech. Phys. Lett., **36** (11), 1066 (2010).
[5] W.V. Lundin, A.E. Nikolaev, A.V. Sakharov, E.E. Zavarin, G.A. Valkovskiy, M.A. Yagovkina, S.O. Usov, N.V. Kryzhanovskaya, V.S. Sizov, P.N. Brunkov, A.L. Zakgeimb, A.E. Cherniakov, N.A. Cherkashin, M.J. Hytch, E.V. Yakovlev, D.S. Bazarevskiy, M.M. Rozhavskaya, A.F. Tsatsulnikov. J. Cryst. Growth, **315**, 267 (2011).
[6] D. Li, K. Jiang, X. Sun, C. Guo. Adv. Optics and Photonics, **10** (1), 43 (2018).
[7] Y. Nagasawa, A. Hirano. Appl. Sci., **8** (8), 1264 (2018).
[8] S.M.N. Hasan, W. You, M.S.I. Sumon, S. Arafin. Photonics, **8**, 267 (2021).
[9] P.A. Bokhan, N.V. Fateev, T.V. Malin, I.V. Osinnykh, Dm.E. Zakrevsky, K.S. Zhuravlev. J. Luminesc., **203**, 127 (2018).
[10] I.V. Osinnykh, T.V. Malin, D.S. Milakhin, V.F. Plyusnin, K.S. Zhuravlev. Jpn. J. Appl. Phys., **58**, SCCB27 (2019).
[11] N. Antoine-Vincent, F. Natali, M. Mihailovic, A. Vasson, J. Leymarie, P. Disseix, D. Byrne, F. Semond, J. Massies. Appl. Phys. Lett., **93**, 5222 (2003).
[12] P.A. Bokhan, K.S. Zhuravlev, D.E. Zakrevsky, T.V. Malin, I.V. Osinnykh, N.V. Fateev. Tech. Phys. Lett., **47** (9), 692 (2021).
[13] P.A. Bokhan, N.V. Fateev, T.V. Malin, I.V. Osinnykh, D.E. Zakrevsky, K.S. Zhuravlev. J. Luminesc., **252**, 119392 (2022).
[14] K.L. Shaklee, R.F. Leheny. Appl. Phys. Lett., **18** (11), 475 (1971).
[15] L. Cerdan. Optics Lett., **42**, 5258 (2017).
[16] A.G. Zverev, R.F. Nabiev, A.N. Pechenov, Yu.M. Popov, S.D. Skorbun. Kvantovaya Elektron., **7** (9), 2011 (1980) (in Russian).
[17] P.A. Bokhan, K.S. Zhuravlev, Dm.E. Zakrevsky, T.V. Malin, I.V. Osinnykh, N.V. Fateev. Tech. Phys. Lett., **45** (9), 951 (2019).
[18] I.V. Osinnykh, I.A. Aleksandrov, T.V. Malin, K.S. Zhuravlev. Fiz. Tekh. Poluprovodn., **56** (8), 802 (2022) (in Russian).
[19] M. Lamprechta, K. Thonke. J. Appl. Phys., **123**, 095704 (2018).